Int. J. Electrochem. Sci., 11 **(2016)** 3824 - 3842

International Journal of
ELECTROCHEMICAL
SCIENCE
www.electrochemsci.org

Effect of $[NO_2^-]/[Cl^-]$ Ratio on Corrosion Behavior of Fine-grain High-strength Reinforcement in Simulated Concrete Pore Solutions

Bilan Lin[1,*], *Yuye Xu*[2]

[1] School of Material Science and Engineering, Xiamen University of Technology, Xiamen 361024, China
[2] College of Civil Engineering, Huaqiao University, Xiamen, Fujian 361021, China
[*]E-mail: linbilan@xmut.edu.cn

Received: 19 January 2016 / *Accepted:* 24 February 2016 / *Published:* 1 April 2016

The corrosion behavior of fine-grain high-strength reinforcement (HRBF500 reinforcement) in simulated concrete pore (SCP) solutions with various $[NO_2^-]/[Cl^-]$ ratios was investigated using polarization and electrochemical impedance spectroscopy (EIS) techniques. The semiconductor property of the passivation film was studied via Mott-Schottky curves. The corrosion products on HRBF500 reinforcement were analyzed through SEM and EDS. The corrosion inhibition efficiency of nitrate for HRBF 500 reinforcement was compared with that for the regular carbon steel reinforcement (HPB235 reinforcement). The results show that more chloride ions in SCP solutions lead to serious cracking of the passivation film on HRBF500 reinforcement. In the presence of nitrite, the corrosion resistance improves. The passivation film is a classical n-type semiconductor. However, the corrosion inhibition by nitrite for HRBF500 reinforcement is less than that for HPB235 reinforcement and the etch pits are still observed.

Keywords: reinforcement; fine grain; corrosion; simulated concrete pore solution; nitrite; polarization; electrochemical impedance spectroscopy

1. INTRODUCTION

Popularization and application of high-strength reinforcement in a reinforced concrete structure can bring great economic and social benefits. The grain refining can simultaneously improve the strength and plasticity of the metal. The recent methods to the grain refining for reinforcement are the micro alloying with Nb, V and Ti and the thermo mechanical control processing (TMCP). The TMCP

doi: 10.20964/110383

is a total technology for controlling rolling and controlling cooling [1, 2]. A non-homogeneous microstructure is produced in austenite and thus provides a large number of the nucleation points for ferrite, resulting in a fine grain of ferrite and an enhancement of the obdurability. HRBF500 reinforcement has been newly added into the "Code for Design of Concrete Structures (GB50010-2010)" in China [3], and the strength grade of the dominant stressed reinforcement has been increased to 500 MPa. HRBF is the fine-grain hot-rolled ribbed bar and 500 is the yield strength of the reinforcement.

Corrosion of reinforcement in concrete will lead to a decrease of the section area of reinforcement, an expansion and rupture of the concrete cover, a reduction of the bond strength of the reinforcement/concrete, etc [4-6]. The security, durability and service life of the reinforced concrete structures is thus seriously impaired [7-9]. Corrosion of reinforcement is a complex chemical and electrochemical process that is closely related to the non-uniformity of the microstructure and constituent of the reinforcement and also intimately associated with the nature of the reinforced concrete medium [10-13]. Researches on corrosion and protection of reinforcement in concrete have been mainly focused on HPB235 plain round bar (i.e., regular carbon steel) and HRB335 ribbed bar (i.e., 20MnSi steel) [14-18], while studies on high-strength or fine-grain reinforcement have been rare. Liu *et al* [19] found that the corrosion resistance of Cr modified HRB400 reinforcement in SCP solutions is higher than that of HRB400 reinforcement. Song *et al* [20] achieved a continuous surface nanocrystallization (NC) of rebar by wire-brushing and found that the corrosion resistance of the rebar was significantly improved in Cl^--containing SCP solutions due to an enhanced passivation performance of the NC layer. However, Shi *et al* [21, 22] found that the pitting corrosion resistance of the fine-grain reinforcement in Cl^--containing SCP solutions is inferior to that of the regular carbon reinforcement, depending on the amounts of the grain boundary and the trace elements. In the previous work [23, 24], a preliminary comparison of the corrosion resistance of HRB400, HRB500 and HPB235 reinforcements in carbonated and Cl^--containing SCP solutions was made and found that the former two reinforcements are more sensitive to pH and chloride ions than the latter one.

Passivation film on reinforcement is damaged by the intrusion of chloride ions [25-28]. Corrosion of reinforcement by chloride ions frequently occurs at the coast, in cold place sprinkling salt to ice and in other harsh environments [29, 30]. Corrosion inhibitors for reinforcement are economical and effective and have been widely applied in reinforced concrete structure [31-34]. Nitrite is a desirable anodic corrosion inhibitor and has been obtained a certain popularization and application [35-38]. Qiao *et al* [39] pointed out that the inhibition efficiency of nitrite for reinforcement depends on the molar concentration ratio of nitrite to chloride. HPB235 reinforcement has good corrosion resistance when the $[NO_2^-]/[Cl^-]$ ratio was 0.4 or higher.

In this paper, the effect of $[NO_2^-]/[Cl^-]$ ratio on corrosion of HRBF500 reinforcement in SCP solutions was investigated and the partial results were compared to the results of HPB235 reinforcement in the literature [39].

2. EXPERIMENTAL

2.1 Material and reagent

HRBF500 reinforcement with a diameter of 16 mm was used. The metallurgical structure of HRBF500 and HPB235 reinforcements is shown in Fig.1. Two reinforcements are composed of bright ferrite and grey pearlite. The grain of HRBF500 reinforcement is obviously smaller than that of HPB235 reinforcement.

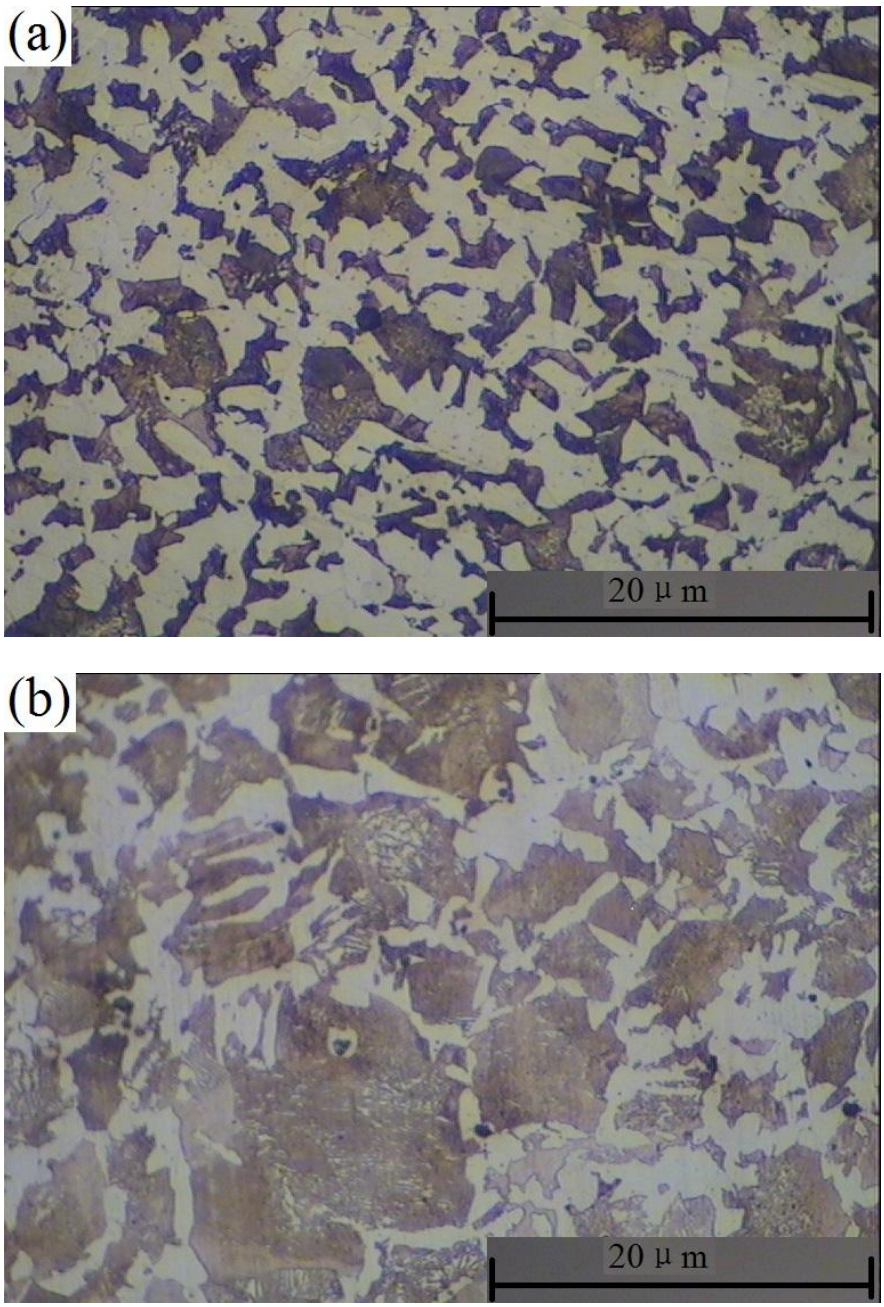

Figure 1. OM images of (a) HRBF500 reinforcement and (b) HPB235 reinforcement

The yield strength and tensile strength of HRB500 reinforcement are 551 MPa and 734 MPa; and those of HPB235 reinforcements are 373 MPa and 506 MPa, respectively.

A saturated calcium hydroxide solution served as the SCP solution and the pH value was about 12.5. Sodium chloride in SCP solutions was 1.0 *wt*.% and 3.5 *wt*.%, so the molar concentration of chloride ions (i.e. [Cl^-]) was 0.171 mol/L and 0.598 mol/L, respectively. Sodium nitrite was also added to SCP solutions to adjust the content of nitrite ions. The [NO_2^-]/[Cl^-] ratio is the ratio of the molar concentration of nitrite ions to that of chloride ions. And it was 0, 0.2, 0.4, 0.8, 1.2 and 2.0, respectively. All reagents were pure analysis, and the de-ionized water was used.

2.2 Electrochemical measurements

Electrochemical measurements were carried out on a CHI760D electrochemical workstation. A common three electrode system was used. A saturated calomel electrode (SCE) served as the reference electrode and a platinum electrode served as the auxiliary electrode. One section of the reinforcement was the working surface with an area of 201.06 mm^2 and other part was mounted with electric jade power. The working surface was first polished with waterproof abrasive paper from grade 200 to grade 2000, and then scrubbed with absolute ethyl alcohol and rinsed with de-ionized water.

Before the electrochemical tests, the reinforcement samples were placed in the testing solutions at room temperature for one hour and a steady open circuit potential was obtained.

The potentiodynamic polarization tests were carried out in the potential range from -0.6 V to 1.2 V with a scan rate of 1 mV/s.

The EIS tests were performed at an open circuit potential and in a frequency range from 100 kHz to 10 mHz and the Zview software was used to fit the EIS diagrams.

The Mott-Schottky curves were tested in a potential range from -0.6 V to 0.6 V with a potential increment of 10 mV, and the frequency and amplitude were 1 kHz and 10 mV, respectively.

There were at least three replicates for each condition. All potential reported in this study was referred to SCE.

2.3 Surface analysis

The morphology and composition of the product layers formed on the surface of HRBF500 reinforcement were analyzed by SEM (EVO-18, ZEISS) and EDS (X- MAX20, OXFORD).

3. RESULTS AND DISCUSSION

3.1 Potentiodynamic polarization curves

Fig. 2 shows the potentiodynamic polarization curves for HRBF500 reinforcement in SCP solutions with various concentrations of chloride ions. In the absence of chloride ions, a stable and broad passivation region on the anodic polarization branch is visible. That is, a stable passivation film is formed on HRBF500 reinforcement in non-contaminated SCP solution.

However, in the presence of chloride ions, the anodic branches are clearly shifted toward the right direction, and the passivation region obviously decreases in the case of containing 0.171 mol/L NaCl and even disappears for the case containing 0.598 mol/L NaCl. This indicates that chloride ions that intrude into the SCP solutions seriously damage the passivation performance of HRBF500 reinforcement.

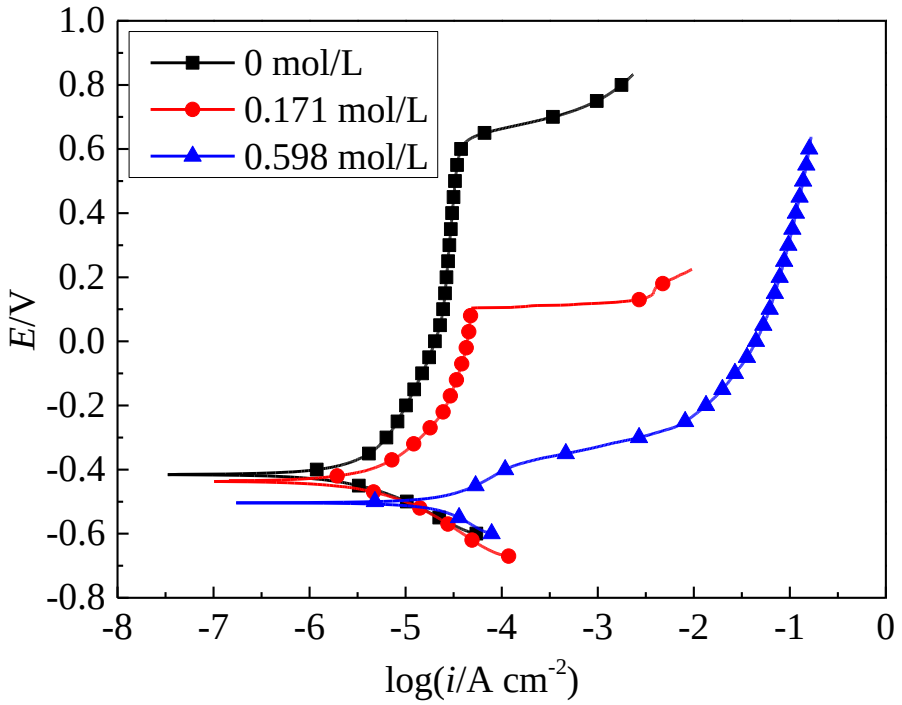

Figure 2. Polarization curves for HRBF500 reinforcement in SCP solutions with different concentrations of chloride ions

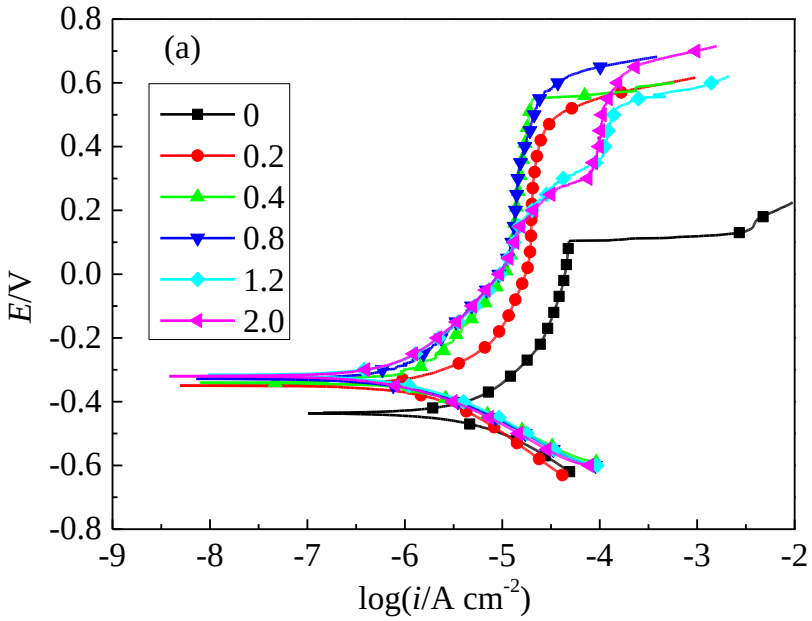

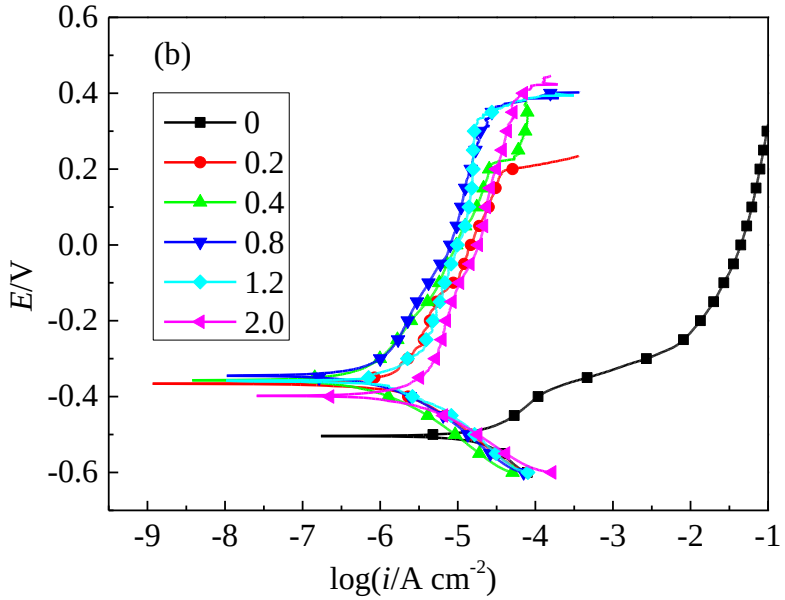

Figure 3. Effect of [NO_2^-]/[Cl^-] ratio on polarization curves for HRBF500 reinforcement in SCP solutions with (a) 0.171 mol/L and (b) 0.598 mol/L NaCl

Fig. 3 shows the effect of [NO_2^-]/[Cl^-] ratio on polarization curves for HRBF500 reinforcement in SCP solutions containing 0.171 mol/L and 0.598 mol/L NaCl. In the presence of nitrite, the cathodic polarization branches are almost unchanged but the anodic branches are significantly shifted leftwards. This also implies that nitrite is an anodic inhibitor [40, 41]. Moreover, the passivation current density decreases and almost all curves exhibit a steady and broad passivation region.

With an increase in [NO_2^-]/[Cl^-] ratio, the extent of the decrease in the passivation current density is initially higher but then decreases. Compared to the case of containing 0.171 mol/L NaCl, the degree of the leftward shift of the anodic branches for containing 0.598 mol/L NaCl is higher.

Table 1. Effect of [NO_2^-]/[Cl^-] ratio on electrochemical parameters for HRBF500 reinforcement in SCP solutions containing 0.171 mol/L NaCl

[NO_2^-]/[Cl^-]	i_{cor}/μA·cm^{-2}	E_{cor}/V	E_b/V	b_c/mV	P_e/%
0	1.20	-0.436	0.104	125	-
0.2	0.414	-0.351	0.467	128	65.5
0.4	0.341	-0.341	0.545	129	71.6
0.8	0.266	-0.328	0.560	123	77.8
1.2	0.197	-0.316	-	121	83.6
2.0	0.202	-0.320	-	121	83.2

Table 2. Effect of $[NO_2^-]/[Cl^-]$ ratio on electrochemical parameters for HRBF500 reinforcement in SCP solutions containing 0.598 mol/L NaCl

$[NO_2^-]/[Cl^-]$	i_{cor}/μA·cm^{-2}	E_{cor}/V	E_b/V	b_c/mV	P_e/%
0	13.2	-0.504	-	123	-
0.2	0.387	-0.366	0.200	132	97.1
0.4	0.199	-0.357	0.212	122	98.5
0.8	0.170	-0.345	0.361	125	98.7
1.2	0.981	-0.358	0.333	124	92.5
2.0	1.01	-0.398	0.400	126	92.3

Tables 1 and 2 list the electrochemical parameters obtained from the polarization curves in Fig.3. i_{cor} is the corrosion current density, E_{cor} is the corrosion potential, and E_b is the breakdown potential of passivation film. b_c is the cathodic Tafel slope. P_e is the corrosion protection efficiency of nitrite for reinforcement and is expressed as $P_e(\%) = (1 - i_{cor}/i_{cor}^0) \times 100$, where i_{cor}^0 and i_{cor} are the corrosion current densities of HRBF500 reinforcement in SCP solutions without and with nitrite, respectively.

As shown in Tables 1 and 2, in the absence of nitrite, i_{cor} of HRBF500 reinforcement in the Cl^--containing SCP solutions is higher, and E_b is very small or even it is un-existent. In the presence of nitrite, i_{cor} is significantly reduced by about one and two orders of magnitude in the case of 0.171 mol/L and 0.598 mol/L NaCl, respectively. E_{cor} and E_b obviously increase, indicating an improvement in corrosion resistance of HRBF500 reinforcement. With an increase in $[NO_2^-]/[Cl^-]$ ratio, i_{cor} initially decreases and then slightly increases, and E_{cor} and E_b firstly increase and then slightly decrease. When the $[NO_2^-]/[Cl^-]$ ratio was 0.8, the corrosion resistance indexes for HRBF500 reinforcement are better.

HRBF500 reinforcement in SCP solutions was passivated except in case of containing 0.598 mol/L NaCl but without nitrite. So the anodic Tafel slope b_a cannot be used to estimate the corrosion rate [42]. However, the cathodic corrosion process of HRBF500 reinforcement in SCP solution is the activation controlled reaction. So b_c can be used [42]. As shown in Tables 1 and 2, b_c in all cases is approximately 120 mV. That is, the cathodic reaction process of HRBF500 reinforcement almost is not changed by the addition of nitrite to SCP solutions. This further indicates that nitrite is an anodic inhibitor.

Moreover, the corrosion inhibition of nitrite for HRBF500 reinforcement in SCP solution containing a higher chloride content (i.e. 0.598 mol/L NaCl) is more effective than that in solution with less chloride (i.e. 0.171 mol/L NaCl). When the $[NO_2^-]/[Cl^-]$ ratio was 0.2, P_e for 0.598 mol/L NaCl and 0.171 mol/L NaCl is 65.7% and 97.1%, respectively. If the $[NO_2^-]/[Cl^-]$ ratio was increased to 0.4, P_e is 71.6% and 98.5%, respectively. These are in good agreement with the results in the literature [39].

A comparison of the corrosion parameters between HRBF500 and HPB235 reinforcements in the literature [39] was made. In the absence of nitrite, i_{cor} for HPB235 reinforcement in SCP solution

containing 0.6 mol/L NaCl was only 2.043 μA·cm^{-2} while that for HRBF500 reinforcement was 13.2 μA·cm^{-2}. When the [NO_2^-]/[Cl^-] ratio was 0.8, i_{cor} for HPB235 reinforcement was 0.0211 μA·cm^{-2}, while that for HRBF500 reinforcement was larger by approximately one order of magnitude, up to 0.170 μA·cm^{-2}. The maximum P_e value for HPB235 reinforcement was 99.5%, higher than that for HRBF500 reinforcement. All these suggest that the corrosion resistance of HRBF500 reinforcement is inferior to that of HPB235 reinforcement when chloride ions were present. And P_e for HRBF500 reinforcement is limited and is smaller than that for HPB235 reinforcement. Therefore the corrosion parameters of HPB235 reinforcement cannot be directly utilized as a durability prediction for HRBF500 reinforcement for a fine-grain high-strength reinforced concrete structure.

3.2 EIS diagrams

Fig. 4 shows the effect of [NO_2^-]/[Cl^-] ratio on EIS diagrams for HRBF500 reinforcement in SCP solutions with 0.171 mol/L and 0.598 mol/L NaCl. The shape of the EIS curves reflects the typical response of all samples in SCP solutions containing chloride ions [23, 32, 41, 43]. In the presence of nitrite, the arc radius and the impedance modulus for HRBF500 reinforcement increase, and the phase angle increases and shifts toward the low frequency direction. With an increase in [NO_2^-]/[Cl^-] ratio from 0.2 to 2.0, the arc radius quickly increases and follows by a small decrease.

The EIS datas were fitted using the typical equivalent circuit depicted in Fig. 5. R_s is the solution resistance. CPE_c and R_c correspond to the first time constant, which is related to the formation of the passivation film or the corrosion product layer on the surface of reinforcement. CPE_c and R_c are the capacitance and the resistance of the formed film, respectively.

CPE_{dl} and R_{ct} correspond to the second time constant and are attributed to the electric double layer at the metal/solution interface, which is normally used to evaluate the charge transfer and the mass transfer processes on the metal surface [32, 43]. CPE_{dl} is related to the double layer capacitance, and R_{ct} is the charge transfer resistance.

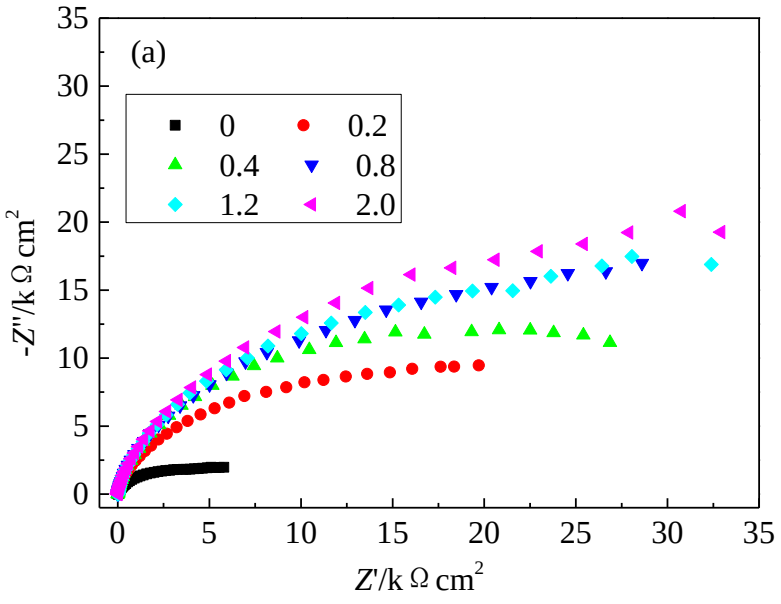

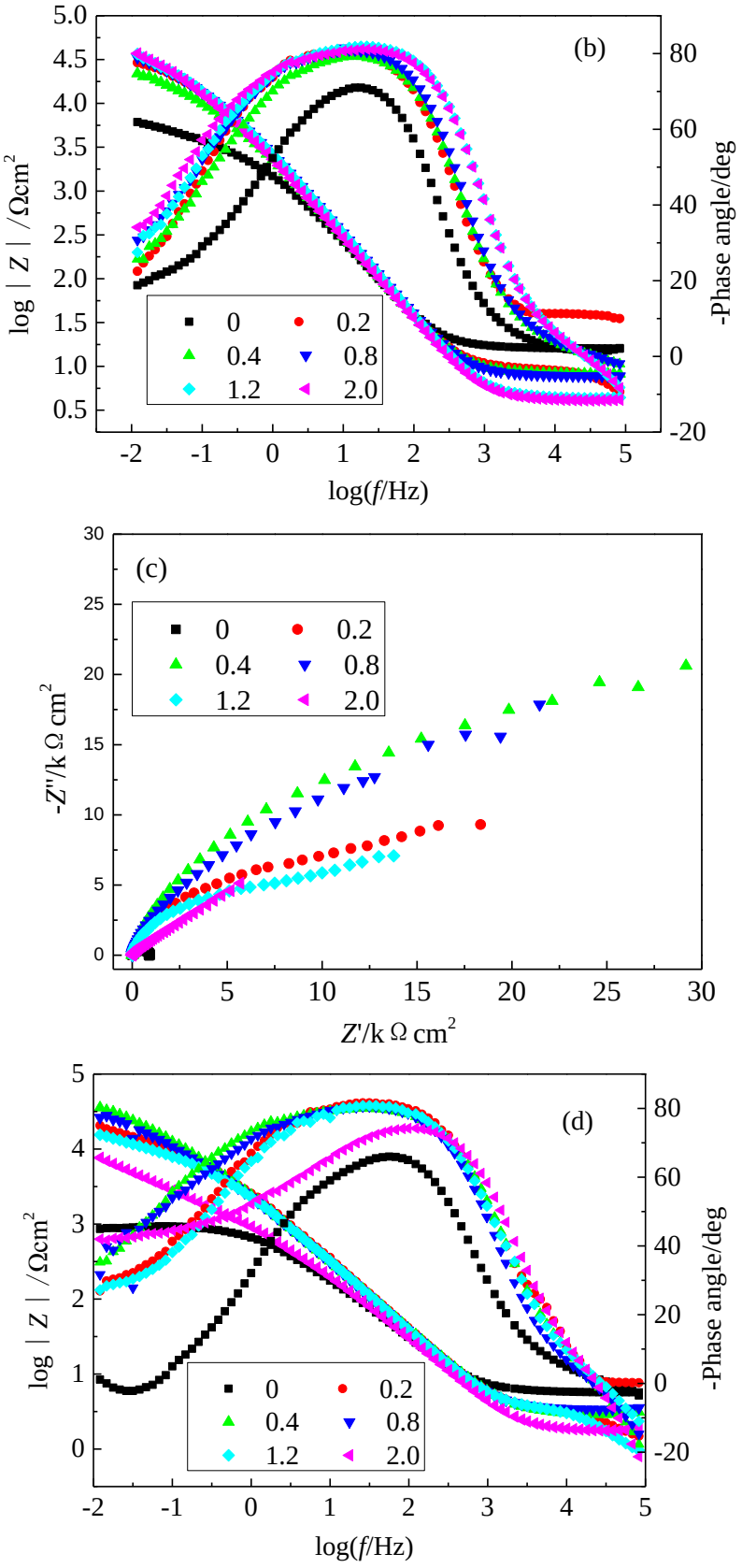

Figure 4. Effect of [NO_2^-]/[Cl^-] ratio on EIS diagrams for HRBF500 reinforcement in SCP solutions: (a) Nyquist diagrams and (b) Bode diagrams with 0.171 mol/L NaCl; (c) Nyquist diagrams and (d) Bode diagrams with 0.598 mol/L NaCl

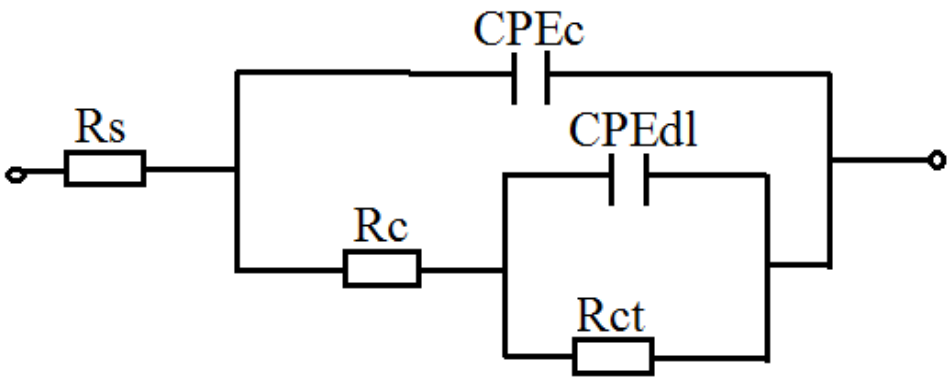

Figure 5. Equivalent circuit for HRB500 reinforcement in SCP solutions

In a practical system the frequency response of the capacitance is changed, manifesting as a depression of the semicircle in Nyquist diagram and a deviation of the phase angle from 90° in Bode diagram [44, 45]. A constant-phase element (CPE) is used to characterize the practical capacitance of the electric double layer and the formed film. CPE has the relationship of $Q=1/Y_0(j\omega)^n$. If n was 1 or 0, CPE represents the capacitance (C) or the resistance (R), respectively. When n was in the range from 0 to 1, it is related to the non-homogeneity and the roughness of the reinforcement surface [32].

Fig. 6 shows the experimental and the fitted curves for HRBF500 reinforcement in SCP solutions with an $[NO_2^-]/[Cl^-]$ ratio of 0.2. The fitted curves are in good agreement with the experimental curves, and the fitting error is less than 10%. Thus the proposed equivalent circuit model is feasible.

Tables 3 and 4 show the fitted parameters of the elements in Fig.5 for HRBF500 reinforcement. In the presence of nitrite, R_c and R_{ct} in two Cl^--containing SCP solutions significantly increase, indicating an enhancement of the corrosion resistance of HRBF500 reinforcement. With an increase in $[NO_2^-]/[Cl^-]$ ratio from 0.2 to 2.0, R_c and R_{ct} initially increase and then slightly decrease and the optimum $[NO_2^-]/[Cl^-]$ ratio is approximately 0.8. Furthermore, for the same $[NO_2^-]/[Cl^-]$ ratio, the increase magnitude of R_c and R_{ct} in SCP solutions containing 0.598 mol/L NaCl is higher than that in solution containing less chloride ions. This is consistent with the results of the polarization tests.

Tables 3 and 4 also show the changes of Y_0 and n with $[NO_2^-]/[Cl^-]$ ratio. In the presence of nitrite inhibitor, Y_0 decreases and n increases, which suggests that a passivation film is formed on HRBF500 reinforcement and the roughness of the film is lower, so the frequency response of CPE_c is closer to that of a pure capacitor for which n_c is close to 1.0. Moreover, n_{dl} approaches to 0.5 which indicates that oxygen diffusion plays an increasingly important role in controlling the electrochemical reaction process of the reinforcement [44].

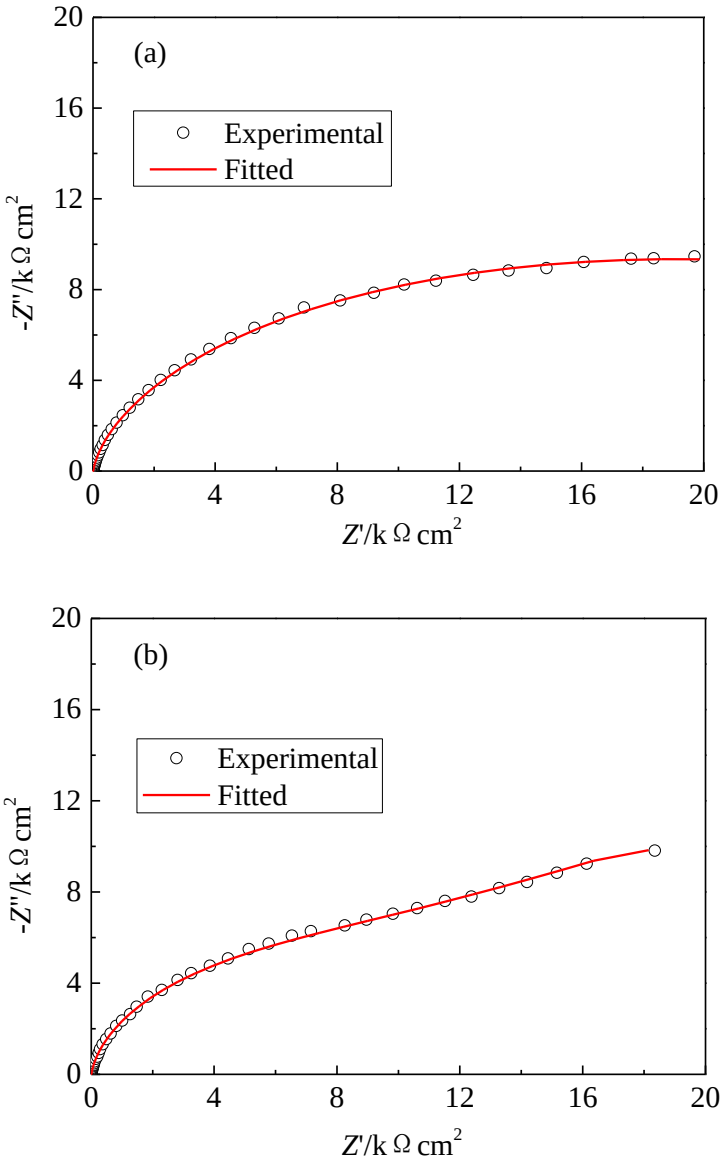

Figure 6. Comparison of the experimental and the fitted curves for HRBF500 reinforcement in SCP solutions with an $[NO_2^-]/[Cl^-]$ ratio of 0.2: **(**a) 0.171 mol/L and (b) 0.598 mol/L NaCl

Table 3. Fitted parameters for HRBF500 reinforcement in SCP solutions containing 0.171 mol/L NaCl and various $[NO_2^-]/[Cl^-]$ ratios

$[NO_2^-]/[Cl^-]$	R_s/ ($\Omega \cdot cm^2$)	R_c/ ($k\Omega \cdot cm^2$)	$Y_{0\text{-}c}$/ ($10^5 \cdot \Omega^{-1} \cdot cm^{-2} \cdot s^{-n}$)	n_c	R_{ct}/ ($k\Omega \cdot cm^2$)	$Y_{0\text{-}dl}$/ ($10^4 \cdot \Omega^{-1} \cdot cm^{-2} \cdot s^{-n}$)	n_{dl}
0	16.2	0.62	8.17	0.913	21.07	2.67	0.278
0.2	8.3	4.84	7.06	0.927	40.48	0.97	0.440
0.4	9.3	6.33	6.80	0.928	59.11	1.04	0.563
0.8	7.8	7.02	6.32	0.936	87.02	0.66	0.416
1.2	4.3	5.65	6.20	0.941	67.43	0.54	0.441
2.0	4.1	5.73	6.79	0.938	86.49	0.45	0.416

Table 4. Fitted parameters for HRBF500 reinforcement in SCP solutions containing 0.598 mol/L NaCl and various [NO_2^-]/ [Cl^-] ratios

[NO_2^-]/[Cl^-]	R_s/ ($\Omega\cdot cm^2$)	R_c/ ($k\Omega\cdot cm^2$)	$Y_{0\text{-}c}$/ ($10^5\Omega^{-1}\cdot cm^{-2}\cdot s^{-n}$)	n_c	R_{ct}/ ($k\Omega\cdot cm^2$)	$Y_{0\text{-}dl}$/ ($10^4\Omega^{-1}\cdot cm^{-2}\cdot s^{-n}$)	n_{dl}
0	5.7	0.31	10.8	0.892	0.64	1.68	0.282
0.2	3.1	5.94	6.20	0.927	30.87	1.54	0.432
0.4	3.0	5.06	6.14	0.932	56.37	0.47	0.391
0.8	3.4	6.67	5.98	0.947	49.85	0.71	0.399
1.2	3.1	6.04	6.82	0.922	24.24	1.86	0.690
2.0	1.8	4.64	8.11	0.926	15.00	3.92	0.435

3.3 Mott-Schottky curves

Generally, the passivation film on the electrode surface has semiconductor characteristics. On the basis of the Mott-Schottky theory [23, 46], semiconductors obey a relationship expressed as

$$\text{n-type: } \frac{1}{C_{sc}^2}=\frac{2}{\varepsilon_0\varepsilon e N_D}\left[E-E_{fb}-\frac{kT}{e}\right]$$

$$\text{p-type: } \frac{1}{C_{sc}^2}=-\frac{2}{\varepsilon_0\varepsilon e N_A}\left[E-E_{fb}-\frac{kT}{e}\right]$$

Where C_{sc} is the capacitance of the space charge layer of the passivation film in the depletion state, E is the electrode potential, ε_0 is the vacuum dielectric constant (8.854×10^{-12} F/m), ε is the relative dielectric constant of the passivation film (it is about 12 for iron oxides [23]), e is the electron charge (1.602×10^{-19} C), N_A and N_D are the donor and acceptor concentrations of the passivation film, respectively. E_{fb} is the flat band potential, k is the Boltzmann constant (1.38066×10^{-23} J/K), and T is the thermodynamic temperature. kT/e is approximately 25 mV at room temperature, so it is neglected in the above two formulas.

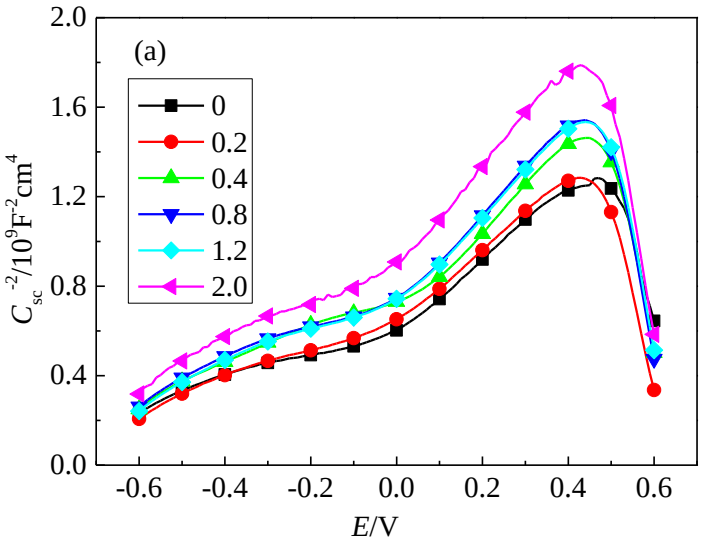

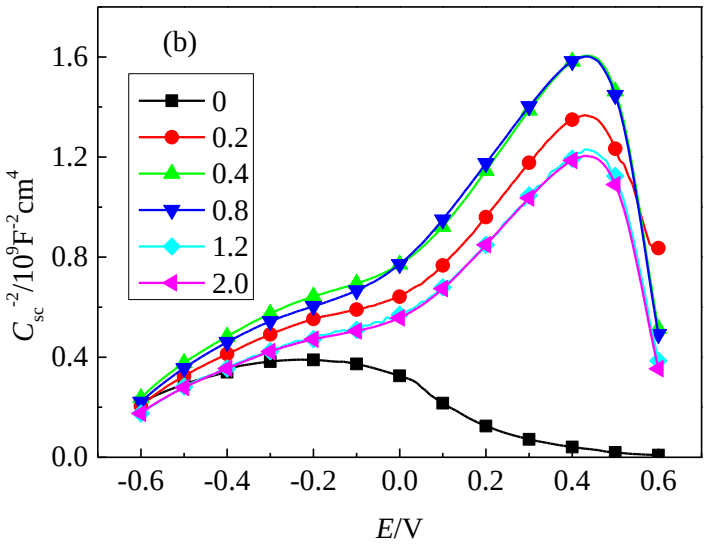

Figure 7. Effect of $[NO_2^-]/[Cl^-]$ ratio on Mott-Schottky curves for HRBF500 reinforcement in SCP solutions with **(**a) 0.171 mol/L and (b) 0.598 mol/L NaCl

Table 5. N_D and E_{fb} of the passivation film on HRBF500 reinforcement in SCP solutions containing 0.171 mol/L NaCl and various $[NO_2^-]/[Cl^-]$ ratios

$[NO_2^-]/[Cl^-]$	-0.6~-0.1/V		0~0.4/V	
	$N_{D1}/(\times 10^{20}cm^{-3})$	E_{fb1}/V	$N_{D2}/(\times 10^{19}cm^{-3})$	E_{fb2}/V
0	1.707	-0.960	7.050	-0.355
0.2	1.433	-0.938	6.645	-0.303
0.4	1.363	-0.851	5.874	-0.286
0.8	1.256	-0.896	5.960	-0.351
1.2	1.242	-0.924	5.853	-0.364
2.0	1.260	-0.984	5.203	-0.373

When the slope of the linear section of a Mott-Schottky curve is positive, the passivation film is n-type semiconductor. Conversely, it is p-type semiconductor. N_A and N_D can be obtained by the slope, and E_{fb} can be obtained by the intercept.

Fig. 7 shows the Mott-Schottky curves for HRBF500 reinforcement in SCP solutions. The slope of the Mott-Schottky curves is positive so the passivation film on the surface of HRBF500 reinforcement displays as an n-type semiconductor. The curves are composed of two line segments, at a low potential interval (-0.6~-0.1V) and a high potential interval (0~0.4V), respectively, which implies that the passivation film is characterized by two donor concentrations [47]. The low potential interval is related to the shallow donor concentration N_{D1}, for which the oxygen hole and Fe^{2+} are the main carriers. Differently, the high potential interval corresponds to the deep donor concentration N_{D2},

for which the oxygen hole and Fe^{3+} are the main carriers. The oxygen hole, Fe^{2+} and Fe^{3+} can participate in the electron transfer [47].

Table 6. N_D and E_{fb} of the passivation film on HRBF500 reinforcement in SCP solutions containing 0.598 mol/L NaCl and various $[NO_2^-]/[Cl^-]$ ratios

$[NO_2^-]/[Cl^-]$	-0.6~-0.1/V		0~0.4/V	
	$N_{D1}/(\times 10^{20} cm^{-3})$	E_{fb1}/V	$N_{D2}/(\times 10^{19} cm^{-3})$	E_{fb2}/V
0	2.034	-0.980	-	-
0.2	1.514	-0.901	6.048	-0.382
0.4	1.218	-0.871	5.353	-0.307
0.8	1.398	-0.816	5.553	-0.311
1.2	1.657	-0.894	6.812	-0.278
2.0	1.964	-0.971	6.689	-0.270

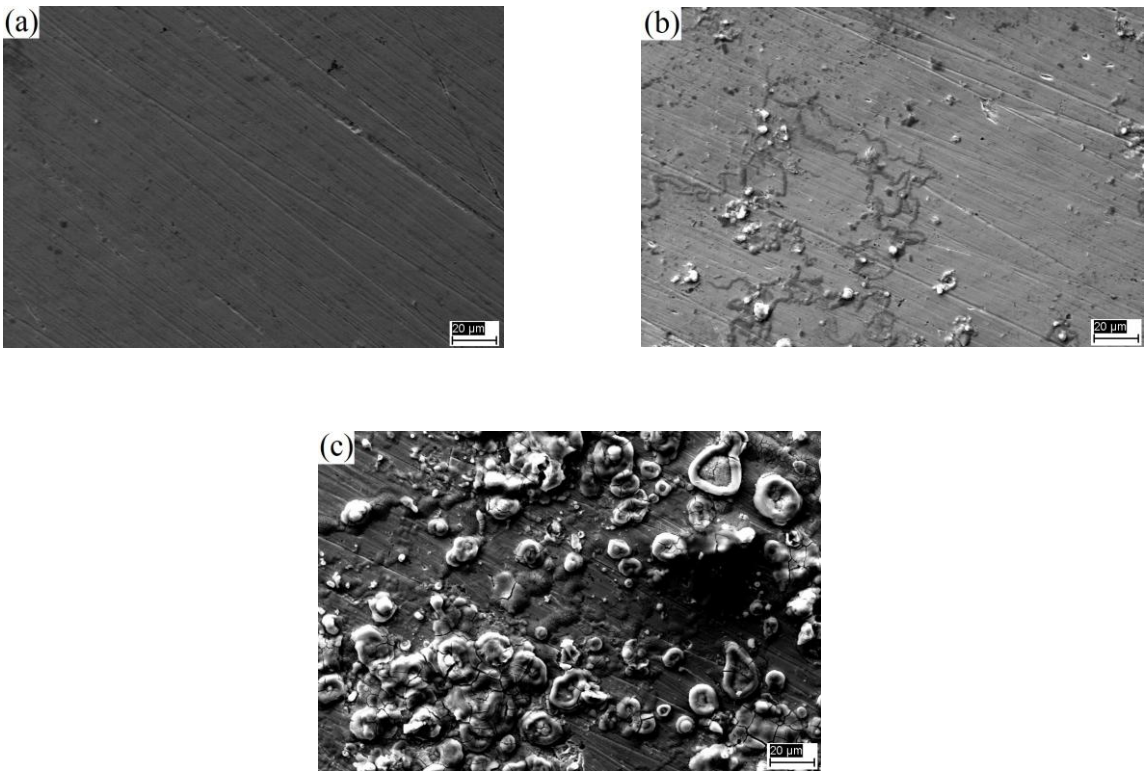

Figure 8. SEM images (at low magnification) of HRBF500 reinforcement in SCP solutions with (a) 0 mol/L, (b) 0.171 mol/L and (c) 0.598 mol/L NaCl

The smaller the donor concentration, the larger the transfer resistance of the electron in the passivation film is and thus the more difficult the reinforcement is to corrode. It should be pointed out that when the NaCl content was 0.598 mol/L and in the absence of nitrite, the line segment at high

potential interval disappears, and suggesting that Fe^{3+} is absent and the corrosion products may be the Fe-O-Cl compounds [47].

Tables 5 and 6 show the N_D and E_{fb} of the passivation film. In the presence of nitrite, both N_{D1} and N_{D2} decrease, implying an enhancement of the compactness of the passivation film and the corrosion resistance of the reinforcement. With an increase in $[NO_2^-]/[Cl^-]$ ratio, N_D first decreases and then slightly increases. Moreover, the degree of the decrease in N_D in the case of containing 0.171 mol/L NaCl is generally less than that containing 0.598 mol/L NaCl. All these are close to the results of the polarization and EIS tests.

3.4 Morphological observations

Fig. 8 shows the low magnification SEM images of HRBF500 reinforcement immersed in SCP solutions with different chloride ions for 1 h. In the absence of chloride ions, the surface of HRBF500 reinforcement is clean and smooth, and there are no pitting holes or corrosion products (Fig. 8a). In the presence of 0.171 mol/L NaCl (Fig. 8b), the corrosion products obviously increase. An increase of NaCl to 0.598 mol/L generated a large amount of corrosion products that almost cover the whole surface (Fig. 8c), indicating a severe corrosion damage of the reinforcement. This is similar to the literatures [48, 49]

The effect of chloride ions on SEM images at a higher magnification is presented in Fig.9, and the corresponding compositions of the different micro sites are listed in Table 7. In the absence of chloride ions (Fig. 9a), the passivation film is flat and contains oxygen. In the presence of 0.171 mol/L NaCl (Fig. 9b), there are flat surfaces (site 1), worm spots (site 2) and bright convex points (site 3) on the surface of HRBF500 reinforcement. The flat surfaces contain oxygen but without chloride, similar to the passivation film formed in the pure SCP solution. However, both the worm spots and the bright convex points contain oxygen and chloride, indicating that chloride ions participate in the formation of the passivation film. Moreover, the chloride content on the bright convex points is higher than that on the worm spots, leading to a more serious cracking of the film. In the presence of 0.598 mol/L NaCl (Fig. 9c), the flat surfaces decrease greatly and are still without chloride. The worm spots and bright convex points grow and crack, and the chloride content is up to 17.88 *at*.%.

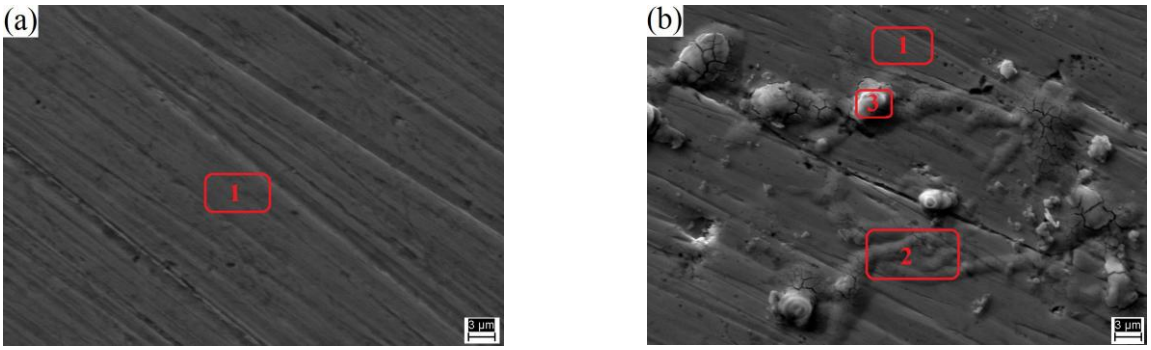

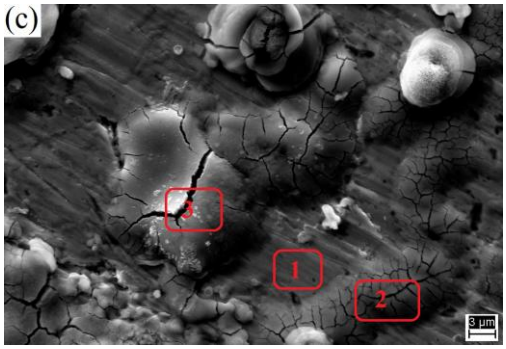

Figure 9. SEM micrographs (at higher magnification) of HRBF500 reinforcement in SCP solutions with (a) 0 mol/L, (b) 0.171 mol/L and (c) 0.598 mol/L NaCl

When chloride ions were not present during the film formation despite the presence of chloride ions in SCP solution, the passivation film formed on HRBF500 reinforcement is flat, smooth and fairly compact. But the cracks are observed when chloride ions involved in the film formation, and the cracking becomes more and more severe as the chloride content increases, leading to a larger N_D of the passivation film (Tables 5 and 6). Therefore, the corrosion resistance of HRBF500 reinforcement is obviously less at a higher concentration of chloride ions in SCP solution.

Table 7. Chemical compositions of different micro-sites corresponding to Fig.9

NaCl content/mol L^{-1}	Micro-sites	Chemical compositions (*at*.%)				
		O	Cl	Fe	Si	Mn
0	1	8.75	0	88.96	1.18	1.11
0.171	1	3.93	0	93.12	1.35	1.60
	2	16.66	0.07	80.2	1.74	1.32
	3	54.55	0.50	43.35	0.85	0.75
0.598	1	9.04	0	88.25	1.09	1.62
	3	45.32	17.88	35.51	0.72	0.58

Fig. 10 shows the SEM images of HRBF500 reinforcement in SCP solutions with an [NO_2^-]/[Cl^-] ratio of 0.8. In the presence of a suitable nitrite inhibitor, the SEM images depict a clean and smooth surface [49, 50]. Almost no pitting holes and no corrosion products are observed in the case of containing 0.171 mol/L NaCl and only a few pitting holes are formed in the case of containing 0.598 mol/L NaCl. This indicates a decrease in corrosion of HRBF500 reinforcement. The EDS results also show that the flat and smooth surfaces contain oxygen but without chloride, while the pitting holes contain a small amount of chloride, approximately 0.09 *at*.%. In addition, the existence of the pitting holes on the reinforcement surface also implies that nitrite alone cannot completely inhibit the corrosion of HRBF500 reinforcement in the Cl^--containing SCP solutions. Therefore, it is necessary to further study other corrosion inhibitors for HRBF500 reinforcement that are more effective and environmentally friendly.

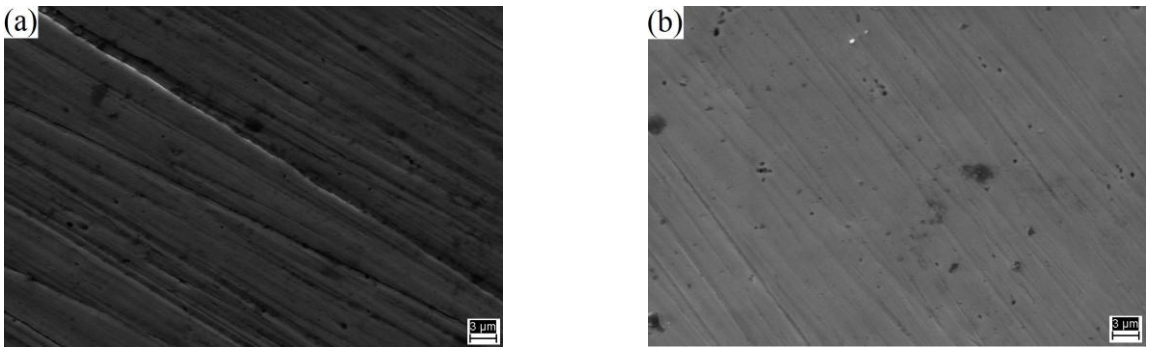

Figure 10. SEM micrographs of HRBF500 reinforcement in SCP solutions with an $[NO_2^-]/[Cl^-]$ ratio of 0.8: **(**a) 0.171 mol/L and (b) 0.598 mol/L NaCl

4. CONCLUSIONS

The corrosion behavior of HRBF500 reinforcement in SCP solutions with various $[NO_2^-]/[Cl^-]$ ratios was investigated. A higher concentration of chloride ions (0.598 mol/L NaCl) in SCP solution leads to a serious cracking of the passivation film and a poor corrosion resistance of HRBF500 reinforcement. In the presence of nitrite inhibitor, the corrosion resistance of HRBF500 reinforcement improves. With an increase in $[NO_2^-]/[Cl^-]$ ratio, the electrochemical indexes first quickly increase and then become nearly stable. The inhibition efficiency of nitrite for HRB500 reinforcement in SCP solutions containing a larger amount of chloride ions is higher than that in solutions containing less chloride ions. The passivation film displays classical n-type semiconductor characteristics. However, the corrosion of HRBF500 reinforcement cannot be completely inhibited by nitrite alone and the etch pits are still observed. The corrosion inhibition for HRBF500 reinforcement by nitrite is inferior to that for the regular carbon steel reinforcement. Therefore, the corrosion performance of HRBF500 reinforcement must be thoroughly investigated due to the wide applications.

ACKNOWLEDGEMENTS
This work was financially supported by the National Nature Science Foundation of China (no. 51408517, 51578255).

References

1. X. W. Kong, L. Y. Lan, Z. Y. Hu, B. Li, T. Z. Sui, *J. Mater. Process. Tech.*, 217 (2015) 202.
2. X. H. Xue, Y. Y. Shan, L. Zheng, S. N. Lou, *Mater. Sci. Eng.: A*, 438-440 (2006) 285.
3. 'Code for design of concrete structures [S]', GB50010-2010, Beijing, China, 2010.
4. W. J. Zhu, R. François, D. Coronelli, D. Cleland, *Eng. Struct.*, 56 (2013) 544.
5. A. Bossio, T. Monetta, F. Bellucci, G. P. Lignola, A. Prota, *Cem. Concr. Res.*, 71 (2015) 78.
6. H. Yalciner, O. Eren, S. Sensoy, *Cem. Concr. Res.*, 42 (2012) 643.

7. M. Dogan, *Eng. Fail. Anal.*, 56 (2015) 275.
8. P. Schiessl, *Constr. Build. Mater.*, 10 (1996) 289.
9. S. Ahmad, *Cem. Concr. Compos.*, 25 (2003) 459.
10. Y. S. Ji, G. M. Zhan, Z. C. Tan, Y. J. Hu, F. R. Gao, *Constr. Build. Mater.*, 79 (2015) 214.
11. T. V. Shibaeva, V. K. Laurinavichyute, G. A. Tsirlina, A. M. Arsenkin, *Corros. Sci.*, 80 (2014) 299.
12. P. Ghods, O. B. Isgor, G. J. C. Carpenter, J. Li, G. A. Mcrae, G. P. Gu, *Cem. Concr. Res.*, 47 (2013) 55.
13. B. Pradhan, *Constr. Build. Mater.*, 72 (2014) 398.
14. J. K. Singh, D. D. N. Singh, *Corros. Sci.*, 56 (2012) 129.
15. P. Lu, B. Kursten, D. D. Macdonald, *Electrochim. Acta*, 143 (2014) 312.
16. Y. T. Tan, S. L. Wijesinghe, D. J. Blackwood, *Corros. Sci.*, 88 (2014) 152.
17. Z. H. Dong, W. Shi, X. P. Guo, *Corros. Sci.*, 53 (2011) 1322.
18. J. L. S. Ribeiro, Z. Panossian, S. M. S. Selmo, *Constr. Build. Mater.*, 40 (2013) 40.
19. M. Liu, X. Q. Cheng, X. G. Li, Z. Jin, H. X. Liu, *Constr. Build. Mater.*, 93 (2015) 884.
20. D. Song, A. B. Ma, W. Sun, J. Y. Jiang, D. H. Yang, G. H. Guo, *Corros. Sci.*, 82 (2014) 437.
21. J. J. Shi, W. Sun, G. Q. Geng, *Acta Metall. Sin.*, 47 (2011) 449.
22. J. J. Shi, W. Sun, G. Q. Geng, P. Jiang, *J. Univ. Sci. Technol. Beijing*, 33 (2011) 1471.
23. B. L. Lin, Y. Y. Xu, International Conference on Electronic & Mechanical Engineering and Information Technology, Haerbin, 2011, 5: 2328.
24. Y. Y. Xu, B. L. Lin, *Appl. Mech. Mater.*, 105-107 (2012) 1797.
25. S. Muthulingam, B. N. Rao, *Corros. Sci.*, 93 (2015) 267.
26. B. Pradhan, B. Bhattacharjee, *Constr. Build. Mater.*, 25 (2011) 2565.
27. R. Liu, L. H. Jiang, J. X. Xu, C. S. Xiong, Z. J. Song, *Constr. Build. Mater.*, 56 (2014) 16.
28. H. Yu, K. T. K. Chiang, L. T. Yang, *Constr. Build. Mater.*, 26 (2012) 723.
29. R. E. Melchers, C. Q. Li, *Cem. Concr. Res.*, 39 (2009) 1068.
30. M. A. Pech-Canul, P. Castro, *Cem. Concr. Res.*, 32 (2002) 491.
31. F. L. Fei, J. Hu, J. X. Wei, Q. J. Yu, Z. S. Chen, *Constr. Build. Mater.*, 70 (2014) 43.
32. D. M. Bastidas, M. Criado, V. M. La Iglesia, S. Fajardo, A. La Iglesia, *Cem. Concr. Compos.*, 43 (2013) 31.
33. T. Chaussadent, V. Nobel-Pujol, F. Farcas, I. Mabille, C. Fiaud, *Cem. Concr. Res.*, 36 (2006) 556.
34. H. E. Jamil, A. Shriri, R. Boulif, M. F. Montemor, M. G. S. Ferreira, *Cem. Concr. Compos.*, 27 (2005) 671.
35. A. Królikowski, J. Kuziak, *Electrochim. Acta*, 56 (2011) 7845.
36. H. S. Lee, S. W. Shin, *Constr. Build. Mater.*, 21 (2007) 1.
37. K. K. Sideris, A. E. Savva, *Cem. Concr. Compos.*, 27 (2005) 277.
38. T. A. Söylev, M. G. Richardson, *Constr. Build. Mater.*, 22 (2008) 609.
39. B. Qiao, R. G. Du, W. Chen, Y. F. Zhu, C. J. Lin, *Acta Metall. Sin.*, 46 (2010) 245.
40. P. Garcés, P. Saura, E. Zornoza, C. Andrade, *Corros. Sci.*, 53 (2011) 3991.
41. C. Q. Ye, R. G. Hu, S. G. Dong, X. J. Zhang, R. Q. Hou, R. G. Du: *J. Electroanal. Chem.*, 688 (2013) 275.
42. D. Sachdeva, R. Balasubramaniam, *Corros. Sci.*, 50 (2008) 1340.
43. X. Jing, Y. Wu, *Constr. Build. Mater.*, 25 (2011) 2655.
44. C. N. Cao, J. Q. Zhang, *Electrochemical impedance spectroscopy introduction*, Beijing, Science Press, 2002.
45. L. H. Jiang, G. H. Huang, J. X. Xu, Y. R. Zhu, L. L. Mo, *Constr. Build. Mater.*, 30 (2012) 516.
46. N. B. Hakiki, S. Boudin, B. Rondot, *Corros. Sci.*, 37 (1995) 1809.
47. Q. Wu, Y. Liu, R. G. Du, C. J. Lin: *Acta Metall. Sin.*, 44 (2008) 346.
48. F. M. Tang, H. Xu, W. Chen, R. J. Yang, R. G. Du, C. J. Lin, *J. Funct. Mater.*, 42 (2011) 291
49. X. Zhou, R. Chen, H. Y. Yang, F. H. Wang, *J. Chin. Soc. Corros. Prot.*, 34 (2014) 125

50. J. R. Yang, Y. Guo, F. M. Tang, X. P. Wang, R. G. Du, C. J. Lin, *Acta Phys. -Chim. Sin.*, 28 (2012) 1923.